# Phase diagram of CeVSb_{3} under pressure and its dependence on pressure conditions

E. Colombier, G. Knebel, B. Salce, E. D. Mun, X. Lin, S. L. Bud'ko, and P. C. Canfield

Phys. Rev. B **84**, 064442 — Published 30 August 2011

DOI: 10.1103/PhysRevB.84.064442

# Phase diagram of $CeVSb_3$ under pressure and its dependence on pressure conditions

E. Colombier,[1] G. Knebel,[2] B. Salce,[2] E. D. Mun,[1,3,*] X. Lin,[3] S. L. Bud'ko,[1,3] and P. C. Canfield[1,3]

[1]*Ames Laboratory, Iowa State University, Ames, Iowa 50011, USA*
[2]*SPSMS, UMR-E CEA / UJF-Grenoble 1, INAC, Grenoble, F-38054, France*
[3]*Department of Physics and Astronomy, Iowa State University, Ames, IA 50011, USA*

(Dated: May 27, 2011)

We present temperature dependent resistivity and ac-calorimetry measurements of $CeVSb_3$ under pressure up to 8 GPa in a Bridgman anvil cell modified to use a liquid medium and in a diamond anvil cell using argon as a pressure medium. An initial increase of the ferromagnetic transition temperature $T_C$ with pressures up to 4.5 GPa is observed, followed by decrease of $T_C$ on further increase of pressure and finally its disappearance, in agreement with the Doniach model. We infer a ferromagnetic quantum phase transition around 7 GPa under hydrostatic pressure conditions from the extrapolation to 0 K of $T_C$ and the maximum of the $A$ coefficient from low temperature fits of the resistivity $\rho(T) = \rho_0 + AT^n$. No superconductivity under pressure was observed down to 0.35 K for this compound. In addition, differences in the $T_C(P)$ behavior when a slight uniaxial component is present are noticed and are correlated to the choice of pressure medium.

PACS numbers: 75.50.Cc, 71.27.+a, 75.30.Kz, 74.10.+v

## I. INTRODUCTION

$CeVSb_3$ is a member of the $RVSb_3$ (R=rare-earth) family, with an orthorhombic crystal structure. Two systematic studies[1,2] of this family showed interesting physical properties such as high anisotropy with a quasi two-dimensional crystal structure and different types of magnetic ordering when the rare-earth is changed. Similarly complex properties were also observed in other binary and ternary rare-earth antimonide families, such as $RSb_2$[3], $RCrSb_2$[4] and $RAgSb_2$[5]. $CeVSb_3$ is the only ferromagnetic compound from the $RVSb_3$ family, and has a $T_C$ around 4.6 K[1]. It may be considered a moderately heavy fermion system as its $\gamma$ value is found to be 162 mJ/mol K$^2$ below 2 K[1]. Only a few studies involving this compound have been reported[1,2,6].

Similar ferromagnetic, Ce-based compounds, such as $CeNiSb_3$ or $CeAgSb_2$ were studied under pressure by resistivity measurements[7–9] and they revealed complex phase diagrams with ferromagnetic transitions evolving into antiferromagnetic ones under pressure. Of the Ce-based ferromagnets studied under pressure to date, none have exhibited superconducting behavior.

The reported increase of $T_C$ for applied pressures up to 1 GPa[1] motivated us to continue investigations on $CeVSb_3$ at higher pressures. The expectation was that $T_C$ would pass through a local maximum value and then decrease[10]. Ideally this would present a good opportunity to study possible quantum criticality in a Ce-based ferromagnet. We present here resistivity and ac-calorimetry measurements under pressure up to 8 GPa, in a Bridgman anvil cell modified to use a liquid medium and a diamond anvil cell, respectively. $T_C$ behaves as expected from the Doniach model[10] with an initial increase with pressure up to a maximum above which a fast decrease and eventual disappearance of $T_C$ is observed. The low temperature power law fits of the resistivity are in agreement with the disappearance of the magnetic transition at a quantum critical point.

We observed discrepancies in the $T_C(P)$ behavior between pressure cells using different pressure media and attributed it to the different pressure conditions due to a slight uniaxial stress component existing along the cell axis in the Bridgman anvil cell. Further measurements in the modified Bridgman cell with a different, more hydrostatic, pressure medium, confirmed this assumption. We have also studied the effect of sample orientation on $T_C(P)$, to quantify any dependency on the directions of the uniaxial component of pressure.

## II. EXPERIMENTAL DETAILS

Single crystals of $CeVSb_3$ were grown out of antimony flux as detailed by Sefat *et al.*[1]. Resistivity and specific heat measurements were performed on these crystals up to 7.6 and 6.9 GPa, respectively.

The resistivity samples were measured by a four probe method using the AC-transport option of a Quantum Design Physical Property Measurement System (PPMS) down to 1.8 K or a LakeShore 370 AC resistance bridge with a $^3$He cryostat down to 400 mK. Four, 12.5 $\mu m$ diameter, gold wires were spot-welded to each polished and cut crystal which had typical dimensions of $600 \times 150 \times 40$ $\mu m^3$. Unless otherwise specified, the resistivity was measured along the $c$-axis (the sample largest dimension). The measurement current was 1 mA and the frequency was 17 Hz. Before

each sample was loaded into the pressure cell, the resistivity was measured at ambient pressure on a standard PPMS puck. A reproducible $T_C$ of 4.56 K was deduced from a sharp peak in the derivative of the resistivity, similar to an averaged value of 4.6 K found previously[1].

Before performing studies under pressure, we measured several samples at ambient pressure with current flowing along each of the three crystallographic directions of the orthorhombic structure (at least two samples for each direction). We observed good reproducibility in the resistivity behavior, although the uncertainties associated with measuring the relatively small sample dimensions lead to an error in the resistivity value at room temperature of up to 30-40 % . Each sample's orientation was identified from the crystal's morphology, as was discussed by Sefat *et al.*[1] without any further X-ray Laue measurements. The reproducibility in resistivity from one sample to another was considered an indication that contributions from the other components of the resistivity were low or absent.

In addition, thermal expansion was measured at ambient pressure using a capacitive dilatometer constructed of oxygen-free, high thermal conductivity, copper, mounted in a Quantum Design PPMS instrument. A detailed description of the dilatometer is presented elsewhere[11]. The samples were lightly polished so as to have parallel surfaces which are also approximately parallel to the different crystallographic axis directions. The dimensions range from 0.5 mm to a few mm. Measurements were performed on warming. We define the thermal expansion coefficients as $\alpha_i = \frac{1}{L_i}\frac{dL_i}{dT}$ with $L_i$ being one of the 3 sample's principle crystallographic orientations, and the volume thermal expansion coefficient $\beta = \Sigma(\alpha_i)$.

Resistivity measurements under pressure were performed using a Bridgman cell modified to use with a liquid pressure medium[12,13], either a Fluorinert mixture (1:1 FC70:FC77) or 1:1 n-pentane:isopentane. When not specified, the medium used was 1:1 FC70:FC77. A piece of lead, used as a manometer, and the sample were inserted in a pressure chamber of 1.4 mm inner diameter. The typical transition widths for lead were 15 mK and 40 mK, respectively for 1:1 n-pentane:isopentane and 1:1 FC70:FC77.

Ideally, we would like the pressure to be hydrostatic (i.e. isotropic). However, even with a medium that is a liquid at ambient conditions, the medium freezes at room temperature at some finite pressure and any further application of pressure is expected to give rise to some degree of non-hydrostaticity. As a first approximation, this non-hydrostaticity can be thought of as small uniaxial pressure in addition to a hydrostatic pressure. Given our cell geometry, if a small uniaxial pressure exists, it is anticipated to be in the direction perpendicular to the thin-disk-like sample space volume, i.e. along the cell axis. If we align the sample with one of its crystallographic axes along this direction, then we will say that "pressure is applied along this direction" to identify this potential uniaxial direction. For example, we use in the following the notation $\rho_{c,P//a}$ to refer to the resistivity measured with current along the $c$-axis and with pressure applied along the $a$-axis of the sample.

Although the pressure environment is not perfectly hydrostatic, our results are reproducible. Three samples were measured in a Bridgman cell filled with Fluorinert, current applied along the $c$ axis and pressure along the $a$ axis. The reproducibility of the results was confirmed by the similarity of the *T(P)* phase diagram data.

1:1 n-pentane:isopentane is a medium that is more hydrostatic than 1:1 FC70:FC77 in the Bridgman cell pressure range, as it is known to freeze above 5 GPa at 300 K instead of below 1 GPa for the Fluorinert mixture[14]. However, it is more difficult to handle because of its high compressibility in the low pressure range[15] (below 2 GPa) and because its boiling point is close to room temperature (28.5°C for isopentane). Due to these difficulties, one of the resistivity data sets, in 1:1 n-pentane:isopentane media, was taken in a three wire configuration after the failure of one of the wires. The resulting three wires resistivity measurement gave limited quantitative information, but a sharp transition was still observable, and its derivative, (shown in figure 3.a. below) looks very similar to those obtained from four wires measurements, once the data for the first pressure are scaled to ambient pressure.

The specific heat under pressure was measured in a diamond anvil cell[16,17] up to pressures of 7 GPa and down to 1.5 K, using a $^4$He cryostat. The culet size of the anvils was 0.7 mm. The pressure, changed *in-situ* at low temperatures[16], was read using the ruby fluorescence method. Argon was chosen as a pressure medium. Albeit solidified at 1.4 GPa and 300 K, argon provides close to hydrostatic conditions due to its weak interatomic interactions (i.e it is a very soft solid). Three different pressure runs were performed. For one of these, two pressure cycles were realized by decreasing pressure in one step after a first run with increasing pressure. To perform this measurement, the ac-calorimetry method[17] was used; a quasi-sinusoidal excitation was applied to the sample by a laser via a mechanical chopper. The temperature oscillations of the sample (inversely proportional to the specific heat) were measured with a Au/AuFe (0.07%) thermocouple which was spot-welded onto the sample. We estimated the amplitude of temperature oscillations of the sample $T_{ac}$ from the thermocouple voltage measured $V_{ac}$ and the thermoelectric power of the thermocouple $S_{th}$: $T_{ac} = |V_{ac}|/S_{th}$. In our analysis we assume no pressure dependence of the thermoelectric power of Au:Fe (0.07 %). Furthermore it is impossible to estimate the addenda contribution to the measured signal coming from the pressure cell/medium. Thus, it is impossible to give absolute values of the temperature variation of the specific heat.

## III. RESULTS

### A. Ambient pressure

Our examination of $CeVSb_3$ (space group Pbcm with $a$=13.172 Å, $b$=6.2419Å, $c$=6.0327 Å)[1] under pressure includes the study of the anisotropic properties of $CeVSb_3$ and in particular its sensitivity to slight uniaxial strains. In order to accomplish this, we first investigated the anisotropic resistivity with current $i$ flowing along the three crystalline directions of this compound at ambient pressure (figure 1.a). The resistivity ratios between 300 K and 2 K range from 2, when the current flows along the $a$-axis, to 5.5 along the $b$-axis. The results for current along the $b$ and $c$ axis are consistent with the study from Sefat *et al.*[1], although resistivity values are lower in our measurements. A clear local maximum is observed at around 16 K for $i$ along the $b$-axis, and is barely detected for $i$ along the $c$-axis. A more striking anisotropy is the resistivity measured with current along the $a$-axis, roughly 10 times higher than along the two other directions. The resistivity thus tends to be quasi two-dimensional, and in the following we study the resistivity along the $b$ or $c$ axis, depending on the geometry needed.

In addition, a strong anisotropy in the thermal expansion coefficients is shown in figure 1.b. The broad local maximum of the volume thermal expansion coefficient around 10 K may be related to the Kondo temperature. We applied the Ehrenfest relation for second order phase transitions,

$$\frac{dT_C}{dP_i} = \frac{V_m \Delta\alpha_i T_C}{\Delta C_p} \; ; \; \frac{dT_C}{dP} = \frac{V_m \Delta\beta T_C}{\Delta C_p}$$

where $V_m$ is the molar volume, $\Delta\alpha_i$ and $\Delta\beta$ are respectively a change in the linear or volume thermal expansion coefficients at the phase transition, and $\Delta C_p$ is a change in the specific heat[1] at the phase transition. From this relation, we deduced a substantial uniaxial pressure dependent anisotropy $dT_C/dP_i$ of 0.4 K/GPa, 0.2 K/GPa and 0.7 K/GPa when the pressure is respectively applied along the $a$, $b$ and $c$ axes. The addition of these three components gives $dT_C/dP$=1.4 K/GPa, very close to the low pressure slope $dT_C/dP$=1.2 K/GPa found from the pressure temperature phase diagram (see figure 5 below).

### B. Resistivity under pressure

The primary goal of this study is to investigate the evolution of $T_C$ under pressure. The modified Bridgman cell used with Fluorinert as a pressure medium is known to have a slight uniaxial component in addition to the expected isotropic pressure due in part to its low hydrostatic limit, below 1 GPa. As an example, the iron arsenide superconductors, recently measured with this pressure set-up[13,18], are known to be sensitive to the uniaxial stresses which stabilize the superconducting phase. This superconducting phase is then observed in a broader pressure range of the phase diagram in the presence of a uniaxial component of pressure. $CePd_2Si_2$[19] and $URu_2Si_2$[20,21] are other examples of compounds with strong sensitivity to hydrostatic conditions, although for this last compound, the phase diagram obtained also depends on the quality of the samples. Since $CeVSb_3$ is an orthorhombic compound with clear anisotropy and some degree of electronic correlation, we decided to check its sensitivity to uniaxial component of pressure associated with non-hydrostaticity. The as-grown crystals are relatively large and mechanically sturdy, making them easy to polish to three different geometries to allow for this study. (This is in contrast to iron arsenides, which were soft and easily exfoliated along their tetragonal, $c$-axis.)

The temperature dependent resistivity data of $CeVSb_3$ measured with pressures successively applied along the three crystallographic directions are shown in figure 2. In order to fully investigate the response of the crystal to slight uniaxial stresses, we measured the resistivity along two different directions, but the evolution of the anisotropy of resistivity under hydrostatic pressure was not the main purpose of this work.

In all cases, the resistivity above $T_C$ increases with pressure. $T_C$ itself initially increases with pressure, reaches a maximum value, and then decreases with pressure and finally disappears. The transition is sharp at ambient pressure and broadens progressively. It is difficult to distinguish it as $T_C$ drops towards 0 K. The resistivity curves presented in figures 2.a. and b. are obtained with the same current direction, but the transition temperature increase is slower with pressure in figure 2.b (see *T(P)* phase diagram in figure 5 below). This shows evidence for anisotropy of the pressure response of the crystals, as the reproducibility of results was checked for three pressure runs in similar conditions. For current along the $b$-axis (figure 2.c), the local maximum observed at ambient pressure is still present under pressure; it progressively broadens as it is shifted up to higher temperatures. For each direction of applied pressure, there is a clear and consistent increase of $\rho_{300K}$ over the measured pressure range.

The low temperature resistivity derivative data, $d\rho(T)/dT$, are compared in figure 3, for the three different cell configurations shown in figure 2 as well as an additional cell filled with 1:1 n-pentane:isopentane. The influence of

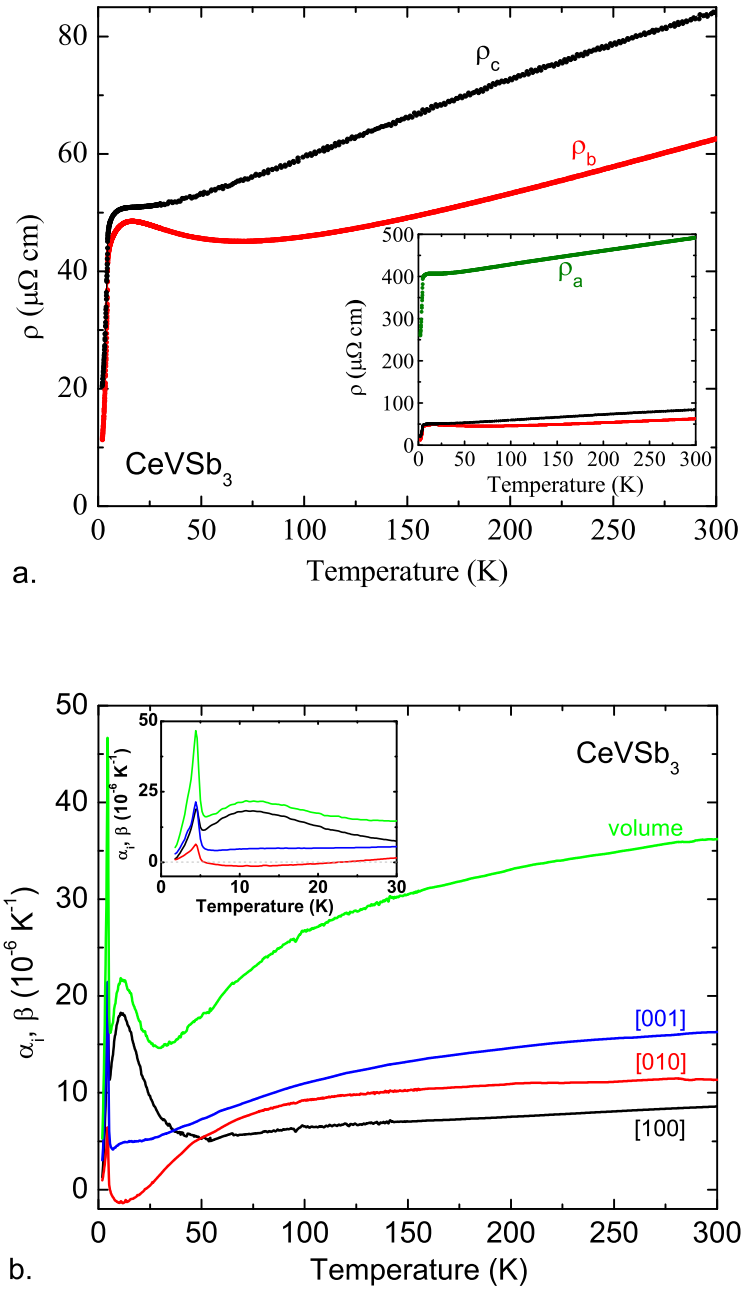


FIG. 1: (Color online) a. Resistivity, at ambient pressure, of $CeVSb_3$ along the $b$ and $c$ axis. The resistivity along the third direction is added to the two other in the inset. b. Anisotropic thermal expansion coefficients of $CeVSb_3$; inset shows expanded, low temperature range.

sample orientation on $T_C$ is even more obvious when the data are presented in this manner. The highest $T_C$ value is observed in fig. 3.d, for the $c$-axis of the sample aligned with the cell axis. In the graphs 3.a and 3.b, the samples' orientations are the same but two different pressure media are used: 1:1 n-pentane:isopentane and 1:1 FC70:FC77, respectively. We observe a strong dependence on pressure conditions. Whereas the feature remains sharp until the highest pressure of 4.5 GPa with 1:1 n-pentane:isopentane (figure 3.a), it has already broadened significantly at a similar pressure in Fluorinert (figure 3.b), and $T_C$ is much lower. In the experiment with Fluorinert, the transition

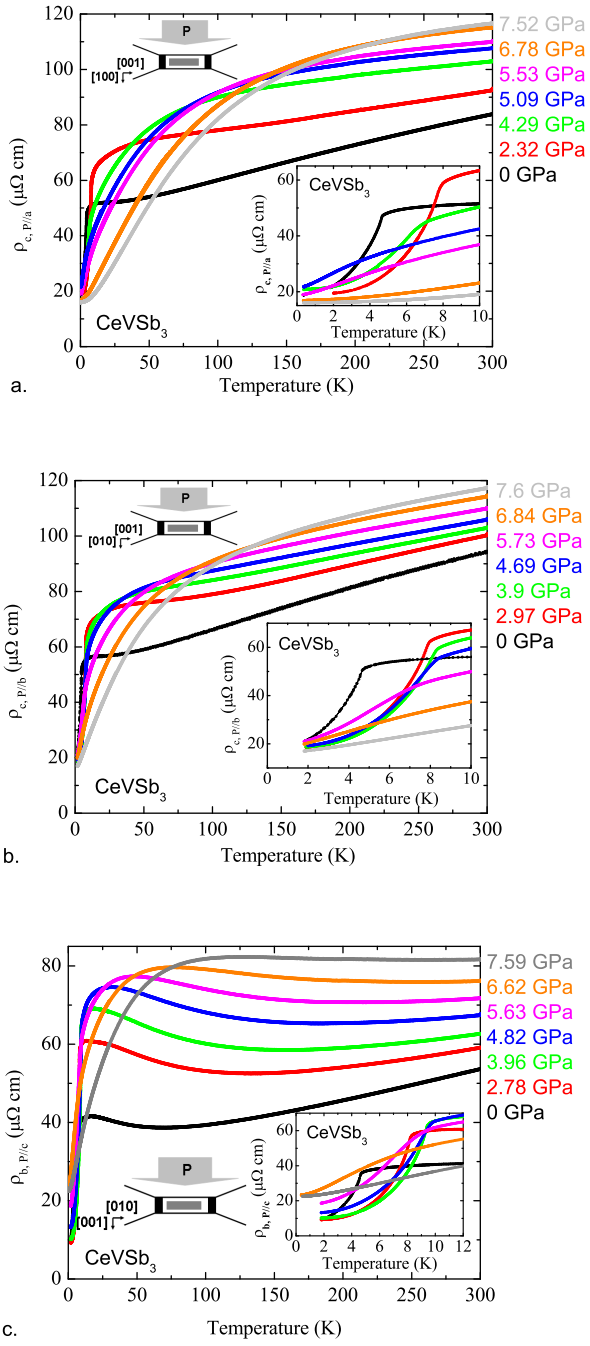


FIG. 2: (Color online) Resistivity measurement of $CeVSb_3$ under pressure. Sketches illustrate the sample orientations in the pressure cells. Insets: low temperature resistivity. a. with current along the $c$-axis and pressure applied along the $a$-axis. b. with current along the $c$-axis and pressure applied along the $b$-axis. c. with current along the $b$-axis and pressure applied along the $c$-axis.

temperature broadens significantly for pressures above 4 GPa.

To further our investigation of the influence of pressure non-hydrostaticity, a noble-gas as a pressure medium was used to provide a near hydrostatic reference. Even when it is solid, its low interatomic interactions indeed allow excellent pressure conditions. This experiment entailed the measurement of specific heat in a diamond anvil cell with argon as a pressure medium, and is described below.

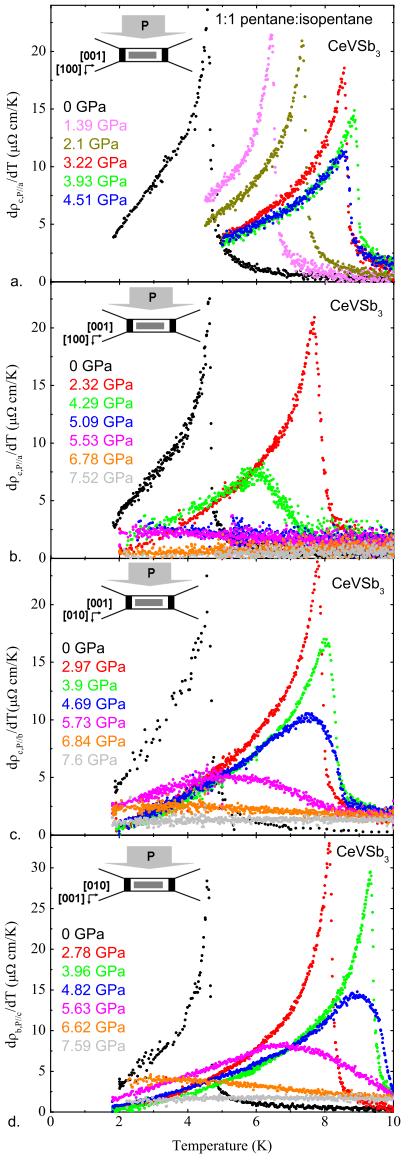


FIG. 3: (Color online) Resistivity derivative $d\rho(T)/dT$ of $CeVSb_3$ under pressure. Sketches outline the sample orientations in the pressure cells. a. with current along the $c$-axis and pressure applied along the $a$-axis in a cell filled with 1:1 n-pentane:isopentane (in $\mu\Omega\ cm/K$ at 0 GPa and arbitrary units under pressure). b. with the same orientation, but filled with 1:1 FC70:FC77 c. with current along the $c$-axis and pressure applied along the $b$-axis with 1:1 FC70:FC77 as a pressure medium. d. with current along the $b$-axis and pressure applied along the $c$-axis with 1:1 FC70:FC77 as a pressure medium.

### C. ac-calorimetry

In figure 4, we present the temperature dependent specific heat curves of $CeVSb_3$ obtained from one of the three pressure runs. The transition at the lowest pressures is sharp with a shape similar to the ambient pressure measurement[1]. The 1.0 GPa $T_C$ value inferred from the data presented in figure 4 is in good agreement with that inferred from the magnetization data at 1.0 GPa[1]. $T_C$ progressively increases with pressure until 4.3 GPa and then decreases. The transition progressively broadens and its amplitude also seems to decrease, although the background and the signal amplitude might be a little different from one measurement to another. Whereas at pressures of 6.0 and 6.3 GPa, a feature is still clearly seen, we can just barely resolve a broad bump in the 6.9 GPa data.

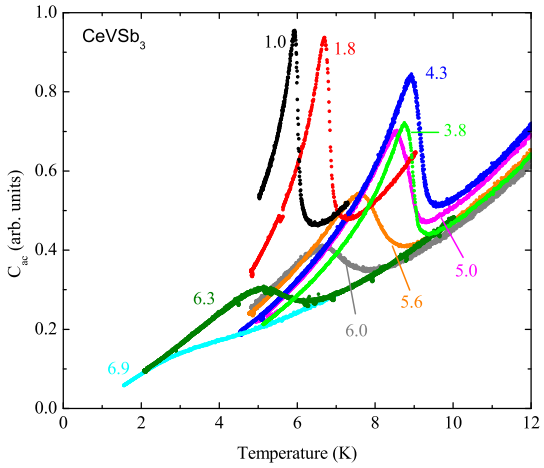


FIG. 4: (Color online) Specific heat of $CeVSb_3$ (in arbitrary units) under pressure, measured in the diamond anvil cell. Pressures are given in GPa.

### D. Phase diagram

Figure 5 shows the phase diagrams obtained from several runs with different pressure conditions and different crystal orientations in the modified Bridgman cell, together with data points inferred from the piston-cylinder cell magnetization data and the diamond anvil cell specific heat data. For each pressure run, we observe a similar dome-shaped phase diagram. However, the data from runs with different media and orientations are somewhat scattered. All curves overlap below at least 2 GPa, however differences in $T_C(P)$ are observed at higher pressures.

We observe obvious differences between the 3 crystal orientations measured in the modified Bridgman cell, figure 5.a. The maximum values of $T_C$ range from 7.9 K to 9.3 K and the corresponding pressures from 3.2 GPa to 4.2 GPa. More importantly, the critical pressure, the pressure at which the $T(P)$ curve extrapolates to zero, ranges from roughly 5.5 to 7 GPa. Since the $T(P)$ curve is reproducible to within 0.3 GPa for three different runs when the cell axis coincides with the $a$ crystallographic axis, we assume any differences between orientations come from an anisotropic response to the slight uniaxial component present in the modified Bridgman cell. This strong anisotropy and sensitivity to uniaxial component of pressure along the $a$ crystallographic axis is confirmed when we use a more hydrostatic pressure medium. Two runs in the modified Bridgman cell with the same crystal orientation (which appears to be the most sensitive to uniaxial pressure) are shown figure 5.b, one with Fluorinert and one with 1:1 n-pentane:isopentane as a pressure medium. Here again we observe differences between the two runs in the maximum value of $T_C$, its corresponding pressure, and the critical pressure. 1:1 n-pentane:isopentane is known to freeze at room temperature above 5 GPa and Fluorinert freezes below 1 GPa[14]. This means that, contrary to the Fluorinert, the 1:1 n-pentane:isopentane was always liquid at room temperature in this experiment, and so was much closer to hydrostaticity. (A conclusion supported by the superconducting transitions widths of the lead manometers, given in the experimental details section.)

The diamond anvil cell filled with argon can be considered as the reference for hydrostaticity since the pressure conditions are presumed to be the best. We observe an increase of $T_C$ from 4.6 K to as high as 9.7 K when the pressure increases from 0 GPa to 4.3 GPa. It then decreases and we expect to have a critical pressure around 7-7.5 GPa. From one run to another, only differences in maximum $T_C$ are noticed. These differences are below 1 K and may be also linked to pressure conditions. Light and medium gray triangles in figure 5 show specific heat measurements from two successive pressure increase in the same diamond anvil cell. We observe a slightly lower maximum $T_C$, around 0.5 K, for the second run, when the sample may be more strained. These differences between runs even with a noble gas as a pressure medium emphasize here again the extreme sensitivity of $CeVSb_3$ to pressure conditions. The diamond anvils cell axis (along which the load is applied) is coincident with the $a$-crystallographic axis of the sample, and the phase diagram is moved up to higher pressures and temperatures, compared to the Bridgman cell measurement using the same sample orientation. Differences between the diamond cell and the Bridgman cell filled with 1:1 n-pentane:isopentane are more subtle and are mainly seen as a lower value of achievable maximum $T_C$ in the Bridgman cell.

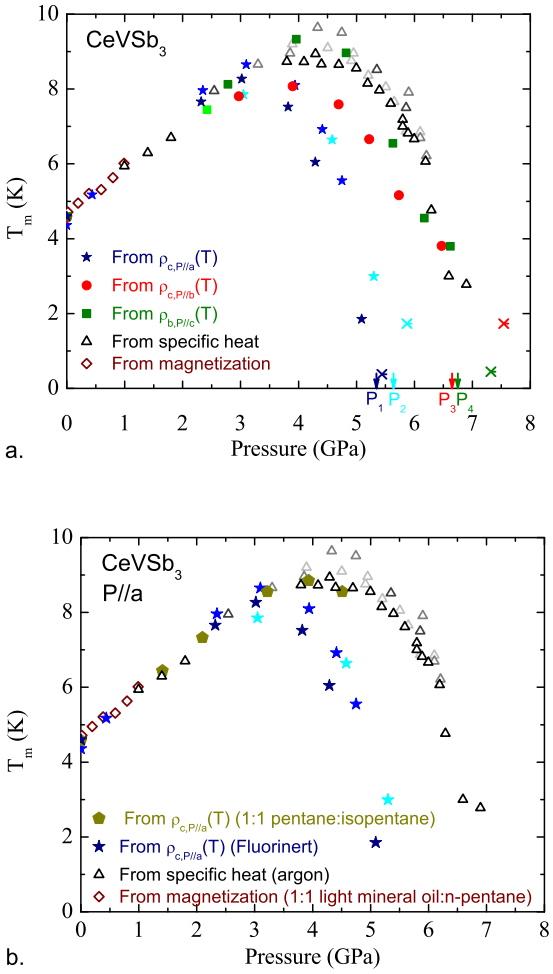


FIG. 5: (Color online) *T(P)* phase diagram of $CeVSb_3$. We added data from magnetization measurements performed in a piston-cylinder cell[1]. For a given symbol, experimental conditions were similar, and the different colors refer to different runs. a. Comparison between the different axis orientations in the Bridgman anvil cell. Diamond anvil cell $C_P$ data points are also shown. Crosses are the lowest measured temperature for the lowest pressure for which no phase transition could be detected. $P_1$, $P_2$, $P_3$ and $P_4$ are given by downwards arrows and refer to the critical pressures estimated from figure 8. b. Comparison between the different pressure media used.

The basic agreement between the 1:1 n-pentane:isopentane data and the $C_p$ data taken in argon and the high pressure deviation of the Fluorinert data from this manifold is further evidence that the discrepancies in the phase diagram can be attributed to an anisotropic sensitivity of the sample to a uniaxial component of pressure. Keeping in mind the strong sensitivity of $CeVSb_3$ to pressure conditions, we try to be very cautious about the impact of pressure conditions in our results.

To estimate the evolution of the samples' sensitivity to pressure conditions, we checked the broadening of the magnetic transition. The lead, as a soft material, is not very sensitive to deviations from hydrostaticity and the broadening of the superconducting transition is modest[13]. The transition broadening of $CeVSb_3$ would indeed be a more obvious clue as long as we are able to estimate contributions from the effects intrinsic to the magnetism. We estimated in figure 6 the broadening of the transition by comparing two different criteria for $T_C$: the maximum of the peak in the $d\rho/dT$ derivative and the onset of this peak from two asymptotes (as shown by dashed lines in the inset). By comparing cells measured in different pressure conditions, we get a good sense of the pressure effect versus the intrinsic properties of the compound. As $d\rho/dT$ appears to be very similar to the heat capacity feature around the transition, the same criteria (shown in the inset of figure 6) were applied to $C_P(T)$ data. This similarity is reminiscent of the work done by Fisher and Langer where the derivative of the magnetic contribution of the resistivity varies like

the magnetic contribution of the specific heat[22].

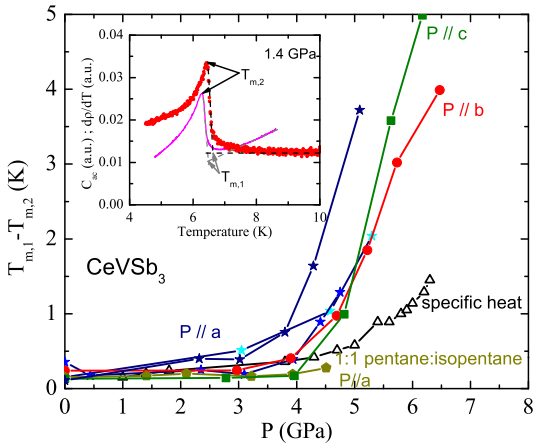


FIG. 6: (Color online) Evolution with pressure of the difference in temperature between two criteria for the magnetic transition. Several curves are shown for different resistivity measurement conditions and one for the specific heat. Three data sets are shown for $P//a$ (stars). The inset shows the definition for these two criteria, for the resistivity derivative and the specific heat.

At ambient pressure, the difference between results using either criteria is around 200 mK in resistivity and it increases only slightly up to around 400 mK at 3 GPa. Above 3 or 4 GPa, the transition broadens strongly, up to a width above 4 K in the modified Bridgman cell filled with Fluorinert. The broadening observed with the 1:1 n-pentane:isopentane set of measurements is at least a factor of two smaller, compared to Fluorinert, with only a slight increase at the highest pressure of 4.5 GPa. The transition measured in specific heat using argon as a pressure medium broadens similarly to the resistivity measurement with the pentane mixture, and the broadening becomes stronger above 5 GPa than below. The transition remains however 2 to 3 times sharper compared to the one measured with a pressure cell filled with Fluorinert. Even though the effect of non-hydrostatic conditions on the transition broadening is obvious, some degree of broadening may be an intrinsic property of the magnetic transition temperature, especially as the slope of $T(P)$ becomes large.

### E. Temperature dependence of low temperature resistivity

Although differences in the pressure dependence are noticed for the several pressure runs shown in the phase diagram in figure 5, the general behavior and in particular the way the magnetic transition is suppressed are similar. As our main interest is to determine if we observe indications of a quantum critical point, we performed further low temperature measurements in a $^3$He cryostat. From these measurements we made low temperature resistivity fits using the equation: $\rho(T) = \rho_0 + AT^n$, where either (i) $n$ equals to 2 or (ii) $n$ was treated as a free fitting parameter. As measurements in a PPMS down to $^4$He temperatures are much more convenient than $^3$He cryostat, we performed only a few measurements down to 0.35 K, so as to check that the fits down to 1.8 K gave qualitatively similar results. Two $^3$He measurements were performed above $P_c$ when the pressure is applied along the $c$-axis of the crystal and another whole set of measurements was made for $P > 3$ GPa with pressure applied along the $a$-axis. We determined the temperature range of the fit either by a progressive increase of the maximum fit temperature, or by checking the linear behavior of $\rho(T) - \rho_0$ versus $T$ on a *log-log* scale, when $\rho_0$ was iteratively, slightly modified. The temperature ranges and fit results obtained from both methods were in good agreement, the maximum fit temperature being up to 3.5-4.0 K for the measurements in a $^4$He cryostat. An example of the fitting using the logarithmic scale is shown figure 7.

The results of fits performed in the $^3$He and in the $^4$He cryostat are in a good qualitative agreement but the parameters values (specifically $n$) can differ of as much as 40% around the critical pressure (where the magnetic transition disappears). Figure 8 presents fit data from when $n$ was left as a free parameter.

The general behavior of $A$ as well as $n$, shown in figures 8.a and 8.b respectively, is similar but shifted in pressure for the three orientations of the sample axes with respect to the cell axis. The $A$ parameter presents a strong peak

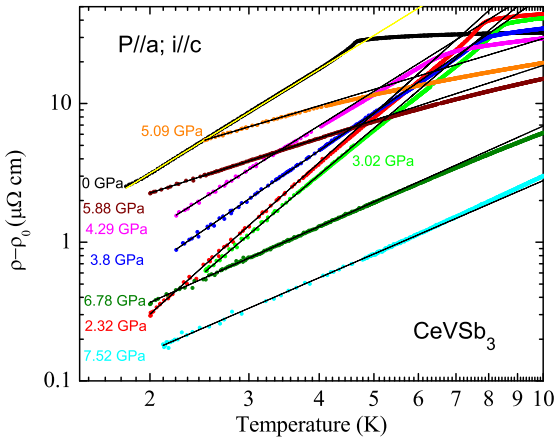


FIG. 7: (Color online) Resistivity of $CeVSb_3$ with the residual resistivity subtracted for each pressure. A logarithmic scale is used for this plot. Linear fits at low temperature are shown for each pressure. This set of data was already shown in figure 2.a.

around the pressure where the magnetic transition disappears. Roughly at the same pressure, a local minimum of the $n$ parameter can be observed. We estimated the critical pressures (labeled $P_1$, $P_2$, $P_3$ and $P_4$ in each panel of figure 8) from the pressure average of the estimated local maximum of $A$ and minimum of $n$. These critical pressures correspond to runs performed using the Fluorinert medium, with $\rho_{c,P//a}$ for $P_1$ and $P_2$ (with the same experimental conditions to check for reproducibility), $\rho_{c,P//b}$ for $P_3$ and $\rho_{b,P//c}$ for $P_4$. The critical pressures obtained this way with fits down to 1.8 K (cf figure 8) were $P_1$ ≈5.3 GPa (+/- 0.2 GPa), $P_2$ ≈5.6 GPa (+/- 0.3 GPa), $P_3$ ≈6.7 GPa(+/- 0.5 GPa) and $P_4$ ≈6.8 GPa(+/- 0.5 GPa). The errors are due to the data spacing and the difference from several fits of $P_c$ estimated from the *T(P)* phase diagram in figure 5.

$\rho_0$ behaves similarly when the cell axis is along the $a$ or $b$ crystallographic axis, with a slight increase around the pressure where $T_C$ disappears and a stronger decrease above. When the cell axis is along the $c$ crystallographic axis, the behavior is different, with a continuous increase which is faster in ∼ 5-7 GPa range of pressures, once $T_C$ decreases. For this orientation, the current is along the $b$-axis, instead of $c$, which may cause a strong pressure dependence in $\rho_0$. The $RRR$ for $\rho_{b,P//c}$ decreases from 7.2 at 0 GPa to 3.5 close to the critical pressure. This is in contrast with the $RRR$ in the two other directions which monotonically increases from 4-5 at 0 GPa to nearly 8 above 7.5 GPa.

Given the essentially complete $\rho_{c,P//a}$ data set from our $^3$He run we can also try forcing the temperature exponent to be exactly equal to two at the lowest temperatures. Figure 9 presents the pressure dependence of $A$ and $\rho_0$ as well as the temperature range over which the $T^2$ fit to the data could be made. These results are consistent with those presented in Figure 8 since there is a divergence in $A$ near 5.1 GPa and the temperature range of the resistivity quadratic behavior drops below our minimum measurement temperature between 5 and 5.5 GPa.

## IV. DISCUSSION

### A. Anisotropy

$RVSb_3$ materials respond anisotropically to chemical and physical pressure. The lattice parameter decrease of $RVSb_3$ is anisotropic when R goes from La to Dy. Sefat *et al.*[1] found a decrease from 0.9% to 5.4% along the $b$ and $a$ axis, respectively. The thermal expansion of $CeVSb_3$ at ambient pressure (figure 1.b) is also clearly anisotropic and we deduced, from the Ehrenfest relation, a uniaxial pressure dependent anisotropy for $T_C$.

These observations motivated us to take advantage of the deviations from hydrostaticity in the modified Bridgman cell, to measure our samples with a slight additional uniaxial pressure component, successively applied along each of the three crystallographic axes. We already observed from figure 5 and 8 that the critical pressure is different depending on the lattice direction along which the pressure is applied. This difference is significantly larger than any cell-to-cell variation. When the uniaxial stresses are applied along a stiffer axis, the crystal may be subject to smaller distortions and a higher pressure would be needed to suppress the magnetic transition. From this picture, the $c$-axis

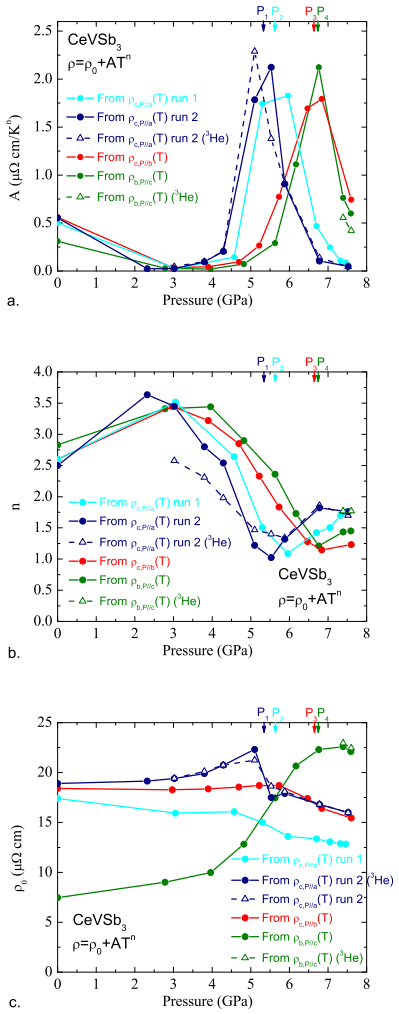


FIG. 8: (Color online) Pressure dependence of the parameters obtained from a low temperature fit $\rho(T) = \rho_0 + AT^n$. The arrows labeled $P_1$, $P_2$, $P_3$ and $P_4$ are the estimated critical pressures (see text) from runs performed using the Fluorinert medium, $\rho_{c,P//a}$ for $P_1$ and $P_2$ (with the same experimental conditions to check for reproducibility), $\rho_{c,P//b}$ for $P_3$ and $\rho_{b,P//c}$ for $P_4$. The triangles refer to fits down to $^3$He temperatures. The colors are chosen the same as in figure 5. a. $A$ coefficient. b. Temperature exponent, $n$. c. Residual resistivity, $\rho_0$.

can be considered as the least sensitive to the Bridgman cell uniaxial component and give results closest to the ones obtained in the more hydrostatic diamond anvil cell.

Whereas the uniaxial pressure dependent anisotropy deduced from the Ehrenfest relation gave us a clue to measure our samples with the pressure applied along several different crystallographic axis, the predicted anisotropy was not retrieved from our measurements at the lower pressures. We do not observe any deviations between the $T_C(P)$ curves below 3 GPa. This might be due to relatively good hydrostaticity in this pressure range.

It is interesting to notice that although deviations in hydrostaticity tend to modify the pressure dependence of $T_C$, the low temperature functional dependence of the resistivity appears to be similar at comparable distances from the critical point. Indeed if we define an effective pressure parameter as $\dfrac{P - P_c}{P_c}$ (with $P_c$, critical pressure determined above) we can plot all of the $A$ and $n$ data on this universal scale (Figure 10). The fact that both the $A$ and $n$ data sets fall onto common manifolds indicates that the quantum critical behavior is inherent to the system and only depends upon the distance from the critical value of the tuning parameter, pressure in this case. This result implies that slight uniaxial components of pressure may be utilized to further tune the criticality without fundamentally changing the underlying physics.

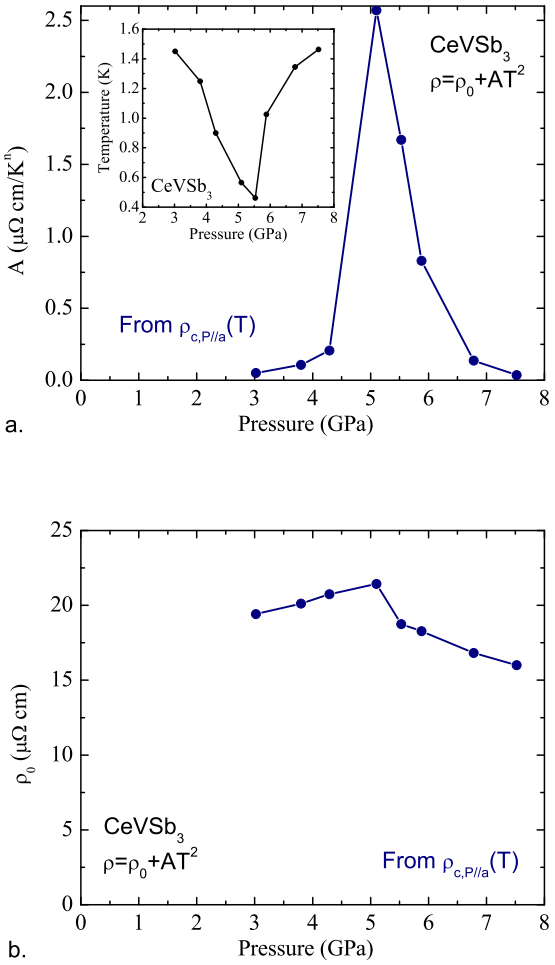


FIG. 9: (Color online) Pressure dependence of the parameters obtained from a low temperature fit $\rho(T) = \rho_0 + AT^2$ from $^3$He data of $\rho_{c,P//a}$. a. $A$ coefficient. The inset shows the maximum temperature where this fit applies. b. Residual resistivity, $\rho_0$.

### B. Phase diagram and possible quantum criticality

When pressure is applied, the magnetic ordering temperature first increases, passing through a maximum before decreasing at a faster rate. No magnetic transition is observed for pressures above 7 GPa. This behavior is consistent with what we expect from the competition between the Kondo effect and the Ruderman-Kittel-Kasuya-Yosida interaction. The phase diagram (figure 5) is in very good agreement with the Doniach model[10].

A goal of this study was to determine the presence of a possible quantum critical point. Although the suppression of $T_C$ seems continuous, we can not clearly follow the transition for $T < 1.5$ K. Even between 1.5 K and at least 4 K, in the modified Bridgman cell as well as in the diamond anvils cell, the peak used to infer the transition temperature is broad and its amplitude is small. This broader transition and lower amplitude may be an additional evidence of the progressive weakening of the magnetic transition once the pressure is high enough to reduce $T_C$, even in good pressure conditions. Furthermore the transition broadening is in part related to the fact that above $\sim 4$ GPa, $T_C(P)$ line is becoming steeper with pressure. The $\Delta T_C$ resulting from fixed experimental uncertainties will consequently increase. In the present case then, it is useful to evaluate the pressure evolution of the fit parameters $\rho(T) = \rho_0 + AT^n$ obtained at very low temperature to find further evidence for a quantum critical point.

As we already showed, it was found to be acceptable to fit only down to 1.8 K ($^4$He cryostat temperatures) at least to get a qualitative behavior. The results from the low temperature fits $\rho(T) = \rho_0 + AT^n$ presented in figures 8 and 10 are consistent with a presence of pressure induced quantum critical point. A sharp peak is observed in the $A(P)$ graph

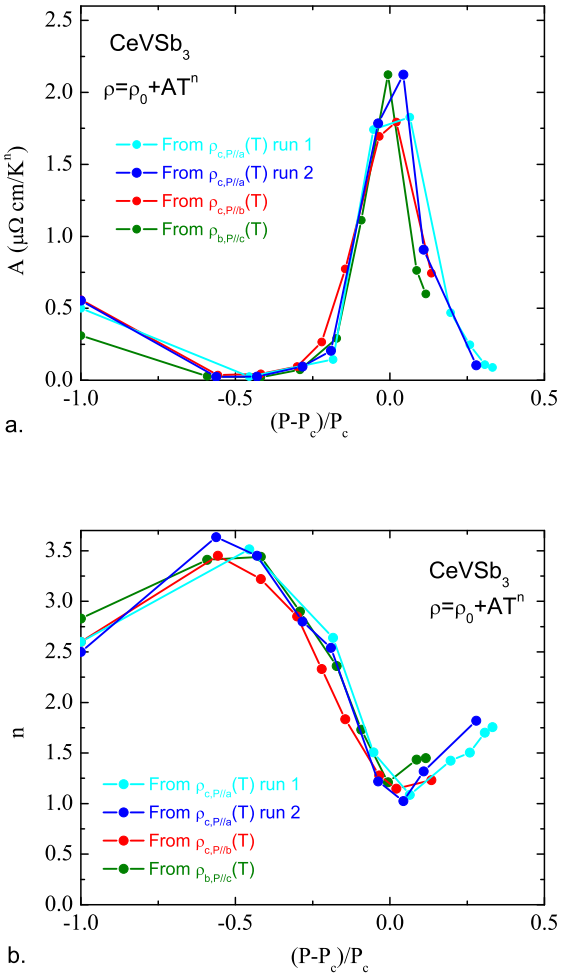


FIG. 10: (Color online) Dependence on a scaled pressure of the parameters obtained from a low temperature fit $\rho(T) = \rho_0 + AT^n$ ($T \geq$1.8 K). The critical pressure values, $P_c$, used here were given in the results section from the low temperature fits of the resistivity. a. $A$ coefficient. b. Temperature exponent, $n$.

and the $n(P)$ graph drops sharply to $n \sim$1 as the critical pressure is approached. At low pressures, the $n$ exponent is above 2 as expected in the magnetic phase for a Kondo lattice system and often observed for other compounds such as $CeRu_2Ge_2$, $YbCu_2Si_2$ and $CeCu_2$[23–25]. This exponent tends to increase with the magnetic transition temperature. It then decreases until the critical pressure. At that point, $n$ is around 1.35-1.4, when measured in a $^3$He cryostat. This value is very close to 4/3, given by the spin fluctuation model in the case of a two-dimensional ferromagnet[26]. However the lowest temperature obtained to determine $n$ was 0.35 K, which might be too high when close to the critical pressure. $n$ is then probably a little underestimated (from our estimations, $n$ tends to increase when the temperature decreases in this pressure range). The $A$ and $\rho_0$ parameters appear to be less sensitive to the fit temperature range. $\rho_0$ slightly increases while approaching $P_c$, and then present a stronger decrease. However, its behavior is much different when pressure is applied along the $c$-axis and current along the $b$-axis, probably because of the resistivity anisotropy. It is interesting to notice that at higher pressures, far enough from the critical pressure, $\rho_0$ is even lower than at ambient pressure.

No superconductivity was observed in this compound down to the lowest temperature of 0.35 K reached in this work. This may be due to the ferromagnetic order, as no superconductivity was found in any other Ce-based ferromagnetic compounds such as $CeNiSb_3$[7] or $CeAgSb_2$[8,9], which had many similarities to $CeVSb_3$. Antiferromagnetic order is indeed known to be more propitious for superconductivity than ferromagnetism[27], and it has been shown that $d$-wave singlet pairing in nearly antiferromagnetic metals is generally much stronger than $p$-wave triplet pairing in nearly

ferromagnetic metals[28]. On the other hand, at least four U-based ferromagnetic compounds, which are all Ising-type ferromagnets, were found to be superconductors, at ambient pressure for URhGe[29] and UCoGe[30], or under pressure for $UGe_2$[31] and UIr[32]. The residual resistivity ratio of $CeVSb_3$ is low (below 10 over the whole pressure range) with a rather high residual resistivity, above 10 $\mu\Omega$ cm, compared to other superconducting Ce compounds. This may evidence a too strong scattering for the occurrence of exotic superconductivity. As an example, the residual resistivity should not be higher than a few $\mu\Omega$ cm in the case of $CePd_2Si_2$ and $CeIn_3$ to observe superconductivity[27]. On the other hand, for the ferromagnet $CeAgSb_2$, no superconductivity was observed in high quality samples with $\rho_0$ below 0.5 $\mu\Omega$ cm[8,9]. In the end, the lowest temperatures reached of 0.35 K might also be too high to observe any eventual superconductivity.

## V. CONCLUSION

We determined the pressure-temperature phase diagram of the ferromagnetic compound $CeVSb_3$. An initial increase of $T_C$ with pressure up to 4.5 GPa (for hydrostatic pressure medium) is observed, followed by the transition being progressively suppressed with further increase of pressure, in agreement with the Doniach model. From the extrapolation of $T_C$ to zero and the low temperature fits of the resistivity, we find a quantum phase transition around 7 GPa. No superconductivity was observed down to 0.35 K. We took advantage of the uniaxial component which is added to hydrostatic pressure in the modified Bridgman anvil cell and successively applied this small pressure component along the three axes. Discrepancies were noticed in the $T_C$ *(P)* behavior when this slight uniaxial component is applied. The *c*-axis seems to be stiff enough not be sensitive to the uniaxial component, and present a behavior in agreement with pressure conditions closer to hydrostaticity.

While the modified Bridgman cell filled with Fluorinert was not suitable by itself to perform this study, it was shown to be very useful to evaluate the anisotropy in the uniaxial pressure dependence of the crystal. The use of 1:1 n-pentane:isopentane brought a strong improvement in pressure conditions and we are currently working to be able to consistently use it up to 8 GPa with the modified Bridgman cell.

### Acknowledgments

This work was performed in part at Ames Laboratory, US DOE, under contract # DE-AC02-07CH11358 (E. Colombier, E. D. Mun, S. L. Bud'ko, and Paul C. Canfield). This project has been supported by the French ANR programs DELICE and CORMAT (G. Knebel, and B. Salce). Part of this work was carried out at the Iowa State University and supported by the AFOSR-MURI grant #FA9550-09-1-0603 (X. Lin, and P. C. Canfield). S. L. Bud'ko was also partially supported by the State of Iowa through the Iowa State University. We would also like to acknowledge Stella Kim (I.S.U.) for her assistance with pressure cells measurements and for providing a critical review of the text.

* Currently at NHMFL-Los Alamos
[1] A. S. Sefat, S. L. Bud'ko, and P. C. Canfield, J. Magn. Magn. Mater. **320**, 120 (2008)
[2] K. Hartjes, W. Jeitschko, and M. Brylak, J. Magn. Magn. Mater. **173**, 109 (1997)
[3] S. L. Bud'ko, P. C. Canfield, C. H. Mielke, and A. H. Lacerda, Phys. Rev. B, **57**, 13624 (1998)
[4] M. Leonard, S. Saha, and N. Ali, J. Appl. Phys. **85**, 4759 (1999)
[5] K. D. Myers, S. L. Bud'ko, I. R. Fisher, Z. Islam, H. Kleinke, A. H. Lacerda, and P. C. Canfield, J. Magn. Magn. Mater. **205**, 27 (1999)
[6] M. D. Vannette, A. S. Sefat, S. Jia, S. A. Law, G. Lapertot, S. L. Bud'ko, P. C. Canfield, J. Schmalian, and R. Prozorov, J. Magn. Magn. Mater. **320**, 354 (2008)
[7] V. A. Sidorov, E. D. Bauer, H. Lee, S. Nakatsuji, J. D. Thompson, and Z. Fisk, Phys. Rev. B **71**, 094422 (2005)
[8] V. A. Sidorov, E. D. Bauer, N. A. Frederick, J. R. Jeffries, S. Nakatsuji, N. O. Moreno, J. D. Thompson, M. B. Maple, and Z. Fisk, Phys. Rev. B **67**, 224419 (2003)
[9] M. Nakashima, S. Kirita, R. Asai, T. C. Kobayashi, T. Okubo, M. Yamada, A. Thamizhavel,Y. Inada, R. Settai, A. Galatanu, E. Yamamoto, T. Ebihara, and Y. Onuki, J. Phys.: Condens. Matter **15**, L111 (2003)
[10] S. Doniach, Physica B **91**, 231 (1977)
[11] G. M. Schmiedeshoff, A. W. Lounsbury, D. J. Luna, S. J. Tracy, A. J. Schramm, S. W. Tozer, V. F. Correa, S. T. Hannahs, T. P. Murphy, E. C. Palm, A. H. Lacerda, S. L. Bud'ko, P. C. Canfield, J. L. Smith, J. C. Lashley and J. C. Cooley, Rev. Sci. Instrum. **77**, 123907 (2006)
[12] E. Colombier and D. Braithwaite, Rev. Sci. Instrum. **78**, 093903 (2007)
[13] E. Colombier, S. L. Bud'ko, N. Ni, and P. C. Canfield, Phys. Rev. B **79**, 224518 (2009)
[14] V. A. Sidorov and R. A. Sadykov, J. Phys.: Condens. Matter **17**, S3005 (2005)
[15] S. K. Kim *et al.*, unpublished
[16] B. Salce, J. Thomasson, A. Demuer, J. J. Blanchard, J. M. Martinod, L. Devoille, and A. Guillaume, Rev. Sci. Instrum. **71**, 2461 (2000)
[17] A. Demuer, C. Marcenat, J. Thomasson, R. Calemczuk, B. Salce, P. Lejay, D. Braithwaite, and J. Flouquet, J. Low Temp. Phys. **120**, 245 (2000)
[18] E. Colombier, M. S. Torikachvili, N. Ni, A. Thaler, S. L. Bud'ko, and P. C. Canfield, Supercond. Sci. Technol. **23**, 054003 (2010)
[19] A. Demuer, A. T. Holmes and D. Jaccard, J. Phys.: Condens. Matter **14**, L529 (2002)
[20] N. P. Butch, J. R. Jeffries, D. A. Zocco, and M. B. Maple, High Press. Res. **29**, 335 (2009)
[21] N. P. Butch, J. R. Jeffries, S. Chi, J. B. Leao, J. W. Lynn, and M. B. Maple, Phys. Rev. B **82**, 060408(R) (2010)
[22] M. E. Fisher and J. S. Langer, Phys. Rev. Lett. **20**, 665 (1968)
[23] H. Wilhelm, K. Alami-Yadri, B. Revaz, and D. Jaccard, Phys. Rev. B **59**, 3651 (1999)
[24] K. Alami-Yadri, H. Wilhelm, and D. Jaccard, Eur. Phys. J. B **6**, 5 (1998)
[25] E. Vargoz, P. Link, D. Jaccard, T. Le Bihan, and S. Heathman, Physica B **229**, 225 (1997)
[26] T. Moriya and K. Ueda, Rep. Prog. Phys. **66**, 1299 (2003)
[27] N. D. Mathur, F. M. Grosche, S. R. Julian, I. R. Walker, D. M. Freye, R. K. W. Haselwimmer, and G. G. Lonzarich, Nature **394**, 39 (1998)
[28] P. Monthoux and G. G. Lonzarich, Phys. Rev. B **59**, 14598 (1999)
[29] D. Aoki, A. Huxley, E. Ressouche, D. Braithwaite, J. Flouquet, J. P. Brison, E. Lhotel , and C. Paulsen, Nature **413**, 613 (2001)
[30] N. T. Huy, A. Gasparini, D. E. de Nijs, Y. Huang, J. C. P. Klaasse, T. Gortenmulder, A. de Visser, A. Hamann, T. Gorlach, and H. v. Lohneysen, Phys. Rev. Lett. **99**, 067006 (2007)
[31] S. S. Saxena, P. Agarwal, K. Ahilan, F. M. Grosche, R. K. W. Haselwimmer, M. J. Steiner, E. Pugh, I. R. Walker, S. R. Julian, P. Monthoux, G. G. Lonzarich, A. Huxley, I. Sheikin, D. Braithwaite, and J. Flouquet, Nature **406**, 587 (2000)
[32] T. Akazawa, H. Hidaka, T. Fujiwara, T. C. Kobayashi, E. Yamamoto, Y. Haga, R. Settai, and Y. Onuki, J. Phys.: Condens. Matter **16**, L29 (2004)